Multi-scale modelling of strongly heterogeneous 3D composite structures using spatial Voronoi tessellation

Bassam El Said[1], Dmitry Ivanov[1], Andrew C. Long[2] and Stephen R. Hallett[1]

[1]*Advanced Composites Centre for Innovation and Science (ACCIS), University of Bristol, Queens Building, University Walk, Bristol, BS8 1TR, United Kingdom.*
[2]*Polymer Composites Research Group, University of Nottingham, University Park, Nottingham NG7 2RD, United Kingdom*

*Corresponding author:
Email: bassam.elsaid@bristol.ac.uk; telephone: +44 (0) 117 33 15651; fax: + 44 (0) 117 331 5719

Abstract

3D composite materials are characterized by complex internal yarn architectures, leading to complex deformation and failure development mechanisms. Net-shaped preforms, which are originally periodic in nature, lose their periodicity when the fabric is draped, deformed on a tool, and consolidated to create geometrically complex composite components. As a result, the internal yarn architecture, which dominates the mechanical behaviour, becomes dependent on the structural geometry. Hence, predicting the mechanical behaviour of 3D composites requires an accurate representation of the yarn architecture within structural scale models. When applied to 3D composites, conventional finite element modelling techniques are limited to either homogenised properties at the structural scale, or the unit cell scale for a more detailed material property definition. Consequently, these models fail to capture the complex phenomena occurring across multiple length scales and their effects on a 3D composite's mechanical response. Here a multi-scale modelling approach based on a 3D spatial Voronoi tessellation is proposed. The model creates an intermediate length scale suitable for homogenization to deal with the non-periodic nature of the final material. Information is passed between the different length scales to allow for the effect of the structural geometry to be taken into account on the smaller scales. The stiffness and surface strain predictions from the proposed model have been found to be in good agreement with experimental results.

The proposed modelling framework has been used to gain important insight into the behaviour of this category of materials. It has been observed that the strain and stress distributions are

strongly dependent on the internal yarn architecture and consequently on the final component geometry. Even for simple coupon tests, the internal architecture and geometric effects dominate the mechanical response. Consequently, the behaviour of 3D woven composites should be considered to be a structure specific response rather than generic homogenised material properties.

1 - Introduction

The increased use of high performance composite materials in a variety of applications requires the adoption of new technologies to improve the performance and reduce the cost of these materials. The drive for better mechanical performance as well as manufacturing efficiency has led to the introduction of composite materials with through-thickness reinforcement produced in a near net-shape pre-form. An example of such a material, is 3D woven composites which are formed from multiple layers of fibre reinforcements woven together with through-thickness binder yarns [1, 2]. The result is a woven fabric preform that can be consolidated, infused with resin and cured into the desired final shape. These materials exhibit enhanced impact performance and energy absorption characteristics [3-5]. However, the presence of binder yarns during weaving introduces localized deformations such as yarn crimp and waviness [6, 7]. Figure [1a, 1b] shows an example of these internal feature on the meso-scale (scale of individual yarns). Additional deformation occurs during the second phase of manufacturing which is the compaction in a mould tool. Unlike the periodic deformations, which are introduced during weaving, the compaction deformation is a result of forming the fibres into the final structural geometric shape. These deformations are thus dependent on the tool geometry and are typically non-periodic in nature. The yarn paths change as the preform is compressed to conform to the tool surface. Additionally, depending on the part final geometry, the preform will experience different levels of compaction at various locations [8]. Figure [1c, 1d] shows an example of such deformations on the sub-component or feature scale. Research has shown that the meso-scopic deformations have a significant impact on 3D woven materials mechanical performance [9]; since, the damage initiation process in these materials is dominated by the stress concentrations associated with this localized deformation. Figure [1e, 1f] shows further examples of such internal features in a 3D woven orthogonal material.

The yarn architecture deformations occurring during forming and compaction, which will be termed “compaction deformation” hereafter, when combined with the internal features present from material weaving, results in a non-periodic highly heterogeneous material with its properties

dependent on the structural geometry. With the help of modelling or experiments the internal yarn architecture of a 3D composite structure can be accurately described. However, this knowledge does not mean that the mechanical behaviour of the final structure can be predicted from finite element models. For conventional solid mechanics problems, it is reasonable to make the separation between the material properties and the structure. The material behaviour is assumed to follow a consistent behaviour throughout certain domains and hence can be represented by an equivalent material model. This kind of separation is not possible for 3D composites since the material behaviour is dependent on the final structural geometry and the manufacturing process. Additionally, for this category of materials, the strain variation at component scale is comparable to the size of the characteristic model building block. For this case, the material mechanical response cannot be measured consistently using coupon testing at a scale larger than that of the composites constituents, which are the yarn and matrix. On the other hand, building detailed models from the ground up including all the details of the yarn architecture for a full scale structure is not possible with the computational power available today or in the near future. Here, the need arises for a multi-scale modelling approach that can link the basic constituents through multiple length scales all the way to the structural scale.

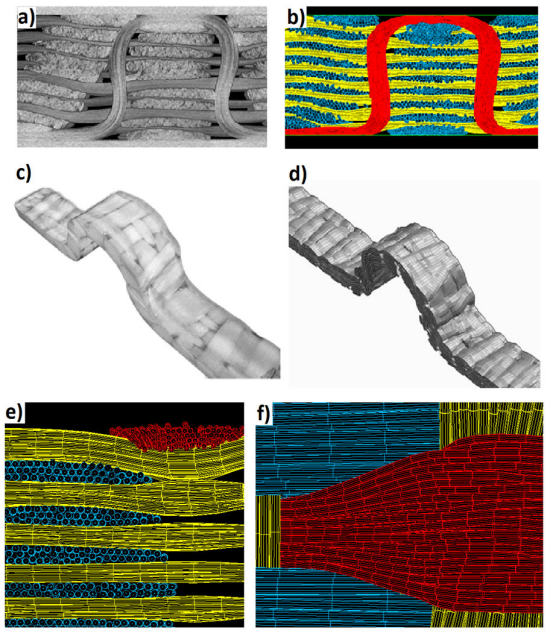

Figure 1. Features and deformations in 3D composites. a) CT-Scan close up on a binder yarn, b) Kinematic model close up on a binder yarn, c) CT- Scan of a finished 3D woven component, d) Deformation model of a cured 3D woven component, e) Deformation model showing yarn waviness, f) Deformation model showing yarn spreading.

Multi-scale approaches have seen wide use in predicting the behaviour of heterogeneous materials. Moreover, several of those multi-scale techniques have been adopted to composite materials [10]. These approaches try to address two main challenges arising from the nature of composite materials. The first challenge is including the effect of the yarn architecture in a macro-scale model of the structural behaviour without having to model the heterogeneities explicitly. This is usually achieved by taking a periodic Representative Volume Element (RVE) extracted from the heterogeneous structure. The boundary conditions on RVE's boundaries can be set under an assumption on how this volume interacts with the rest of the material. Periodicity or symmetry of the strain field at the yarn scale are common assumptions. A set of boundary value problems with these conditions provides homogenised/effective properties [11, 12]. Single or multiple RVEs can be used to represent the various possible heterogeneities' patterns [13]. This category of approaches has been applied successfully to various types of heterogeneous materials and across multiple length scales. Woven materials introduce an additional level of complexity due to the presence of an intermediate level for the heterogeneity which is the yarn/tow level, here termed the meso-scale. Dedicated modelling approaches derived from RVE homogenization have been developed to predict the equivalent mechanical properties of a woven unit cell [7, 14-17]. The underlying assumptions for the RVE approach require that, the heterogeneities or at least the heterogeneities' distribution be periodic [18]. If the structure is irregular or strain field is non periodical, the classical homogenisation framework is not applicable. As shown earlier, for complex geometry 3D woven composite material properties are dependent on both the local tow/yarn architecture and the structural geometry and hence are non-periodic. The results obtained using the RVE approach will thus not be descriptive of the true structural response on the macro-scale.

The other main challenge for multi-scale modelling is the non-linear behaviour of heterogonous materials undergoing progressive damage. Damage initiation at the meso- and micro-scales will progress based on the heterogeneities' patterns and the stress and/or strain state on this scale. The damage will degrade the material on the meso scale, which in turn will impact the global structural behaviour. The interaction between the structure at the macro scale and the damage at the meso- and micro-scales is a nonlinear multi-scale problem. A wide array of multi-scale modelling techniques have been developed for this purpose [19-24]. These techniques utilize some form of domain decomposition where the problem domain is divided into two or more domains. The domains can be completely overlapping, partially overlapping or non-overlapping, based on the multi-scale approach used. The smaller scale models can include progressive damage models and are linked to the macro-scale to ensure that the forces and displacements are compatible between the various scales. The modelling approaches in this category are generally efficient and can handle

the progressive damage problems well. However, for most these approach the problem domain needs to be divided into areas of interest, which are modelled in detail, while the rest of the domain is homogenized. Decomposing the 3D woven structure before the analysis start with no prior knowledge of the stress state is not a sound strategy. The effect of the local features, which are different throughout the structure, on the mechanical performance cannot be assessed before solving the macro-scale structure. On the other hand, having detailed models for all the possible sub domains will lead to unpractical model sizes where the multi-scale modelling approach losses its efficiency in terms of computational loads.

The topic of damage initiation and progression in composite materials has been widely studied in literature. Physically based phenomenological damage initiation models have been proposed and widely applied for both fibre and matrix dominated properties [25-27]. Several continuum damage models based on smeared crack approaches have been proposed for modelling of progressive failure [28-32]. Also, the cohesive zone interface element approach has been used to model delamination and cracking in composite materials [33-36]. XFEM based methods have also been proposed as an efficient approach to modelling crack growth [37] and have been applied to composite materials [38]. The choice of which model or group of models to use with composite materials is largely related to a balance between accuracy and computational efficiency and is still an open research topic. However, all these models share in common that a detailed knowledge of the stresses and strains is required throughout the domain where the damage model is applied. For 3D woven materials a dedicated multi-scale approach that takes into consideration the complexities associated yarn architecture and its interaction at both the meso and macro scales is needed. The key features for a successful modelling approach, which leads to the understanding of the complex multi-scale nature of 3D woven composites are:

- The creation of a new basis of homogenization to replace the absence of the unit cell periodicity.
- Representing the effect of the meso-scopic features on the macro-scale model.
- The ability to locate regions of the problem domain subject to high stress / strain with no prior assumptions as to the whereabouts of these regions within the structure.
- The ability to include detailed meso-scale models with high fidelity at critical locations if required.

2 - Modelling Approach Overview

The primary goal of a solid mechanics problem is the prediction of mechanical behaviour at the macro-scale where the loads are applied and design criteria can be implemented. Hence, it is essential, when only the properties of the micro scale constituents are available, to link all the length scales from the fibre to the structural levels in the models. In the proposed approach, three length scales will be investigated micro, macro and meso. The micro scale is the scale of the fibre where the material properties are known and where the structure geometry has no significant impact on the mechanical behaviour. The primary driver of the mechanical behaviour at this scale is how tightly the fibres are packed together and how much of the material volume is filled by matrix. The fibre packing is expressed by the Intra Yarn Volume Fraction (IYVF). Micro-mechanical models based on different IYVF can be built using analytical methods or Finite Elements (FE) [39, 40]. Based on the IYVF at a given location, a set of equivalent 3D orthotropic material properties can be calculated.

The intermediate scale in this approach is the meso-scale. On the meso-scale, the woven composite structure is described in terms of yarn and matrix materials. The material regions enclosed inside a yarn surface are no longer represented as fibre and matrix but as the homogenized orthotropic equivalent properties, as calculated on the micro-scale for a given IYVF. On this scale, the weave pattern is represented by the yarn paths and yarn cross-sections throughout the fabric. In addition, to the weave pattern and the IYVF, meso-scopic features such as crimp and waviness need to be represented to account for the stress concentration resulting from such features. The third scale is the macro-scale, which is the structure or feature scale. At this scale, the structure geometry is modelled, loads and boundary conditions are applied. Additionally, at the macro-scale, materials are no longer presented as the orthotropic yarn and homogenous matrix but as an equivalent orthotropic material. These macro equivalent material models are calculated from the meso-models for a given sub-domain within the structure. However, since the meso-scopic features are not only a result of the weave pattern but also a result of the structure geometry, the macro and meso scales cannot be separated in the same manner as the separation between the meso and micro-scales.

The multi-scale modelling approach proposed here efficiently handles the modelling of 3D woven structures by solving the problem in two steps. An initial phase where a full scale homogenized mechanical model is generated, taking into account the knowledge of the detailed

yarn architecture and the heterogeneities, hereafter called the macro-scale model. The novel macro-scale mechanical model used in this paper will be presented in section 5. The solution of the macro model is used to determine the critical regions within the structure. Next, these critical regions are replaced with high fidelity models where the yarn architecture and heterogeneities are described in sufficient detail, here after called meso-scale models. The meso-scale models are connected to the macro-scale model using a set of Lagrangian Multipliers. This meso/macro-scale interaction allows information to be passed between the two scales thus allowing for the stress state on the meso-scale to affect the response on the macro-scale. Figure [2] shows the overview of the modelling approach. The proposed approach starts by building a detailed deformation model of the component being studied. Next, relevant properties such as the IYVF and the directions are extracted from the deformation model and submitted as input to the multi-scale mechanical modelling phase.

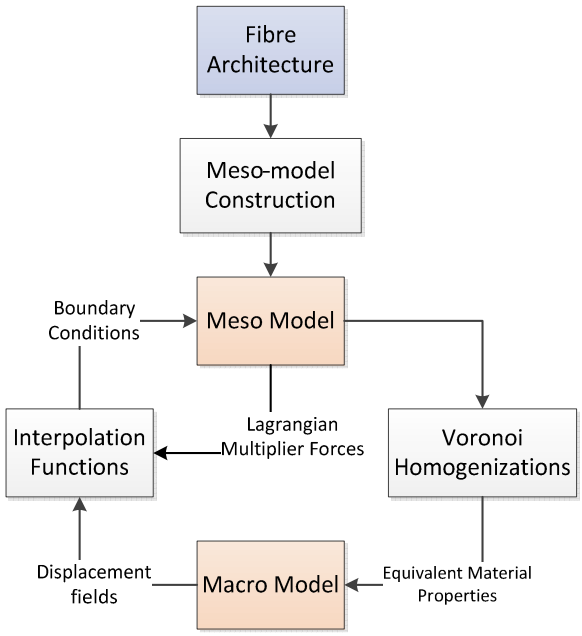

Figure 2. Modelling approach overview

3 - Internal Yarn Architecture

In the proposed modelling framework, the starting point is the meso-scale models, which connects directly from the geometric modelling phase. The meso-scale models are built based on detailed knowledge of the internal yarn architecture at the given location. These meso

models in turn inform the macro models and control the overall structural response. Hence, it is of importance to accurately predict the internal geometry after weaving and compaction. Several approaches have been adopted to determine the yarn geometries of woven materials. These approaches can be classified, based on the formulation used to describe the dry yarn behaviour, into geometric, kinematic and mechanical models. Geometric approaches assume that the yarn behaviour follows that of geometric entities such as splines [41, 42]. A set of geometric rules are used to create the yarn surface geometries ensuring that the yarn paths follow the restriction enforced by the weave pattern and avoiding yarn interpenetration. Such approaches can offer acceptable results for single layer 2D woven materials. However, the coupling of out of plane and in plane deformation in 3D woven fabric create significant challenges for these models that results in less accurate yarn geometries in terms of their path, cross-sections and fibre volume fractions. The geometries calculated using geometric approaches can be enhanced by eliminating yarn interpenetrations in an additional step using contact algorithms [43]. Another approach to eliminate the mechanical modelling mesh quality issues arising from these models is by using mesh superposition approaches. In these approaches the yarn and matrix material are meshed independently [44, 45]. Additionally, experimental data from CT- Scans can be used to augment the geometric approach and considerably enhance the accuracy of such models using direct measurements [46, 47]. The key limitation to using CT-Scan approaches is the need to first manufacture physical samples of the material. Another class of models are kinematic models, where contact algorithms are used to simulate the weaving and compaction of 3D materials. In contrast to the experimental/geometric approach, kinematic models can model the internal yarn architecture with minimal experimental inputs. One notable modelling approach is the Digital Element where each yarn is represented by a bundle of beam elements in a contact model [48-50]. A digital element model under periodic boundary conditions can be used to accurately simulate the weaving deformations. However, the digital element is normally associated with a high computational effort which limits its applicability to the unit cell scale. Another type of kinematic models is the single surface approach which have been specifically developed to handle large scale compaction models [8, 51]. The third category of compaction models is the mechanical models [52-55]. Several constitutive models for representing the mechanical behaviour of dry fibre yarns have been developed and implemented. These models have the advantage of capturing the compaction pressures and forces as well as the final yarn architecture, which is valuable information from a manufacturing engineering point of view. However, the application of these models are still limited to the unit cell scale due to their computational cost.

For calculating the mechanical performance of 3D woven structures, we are only concerned with determining the yarn/weave architecture as an input to the mechanical models. Consequently, kinematic modelling is the optimal approach for predicting the internal yarn geometry. For the large scale models used in this work, a reduced yarn geometric representation is adopted where each yarn is represented by a single surface. Each yarn is divided into a number of connected segments. Each segment is bound by two yarn sections which are defined as polygons. Segments are straight between the two sections and the yarn surface is linearly interpolated between the two sections. An example of how the fabric yarn architecture is defined in this approach is given in Figure [3]. The algorithms described in this section have been applied to a sample of a 3D orthogonal 5 harness satin fabric. The warp yarns have 24,000 fibres each in 8 layers, with 2 yarns per layer of the unit cell. The weft yarns have 12,000 fibres each in 9 layers, with 5 yarns per layer of the unit cell. The binder yarns have 6,000 fibres each. The weft yarn spacing is 5.5 mm and the warp yarn spacing is 2.5 mm. All fibres are 7 μm diameter carbon fibres. The unit cell size of this fabric is 9.9 mm in the weft direction and 27.8 mm in the warp direction. The as-woven thickness is 7 mm and the as-woven volume fraction is 45%. The nominal compacted thickness at 57% volume fraction is 5.5 mm. The composite was woven from carbon fibre and infused using epoxy resin MVR444. The kinematic models for this fabric has been presented and verified against CT-scans by Green et al [7].

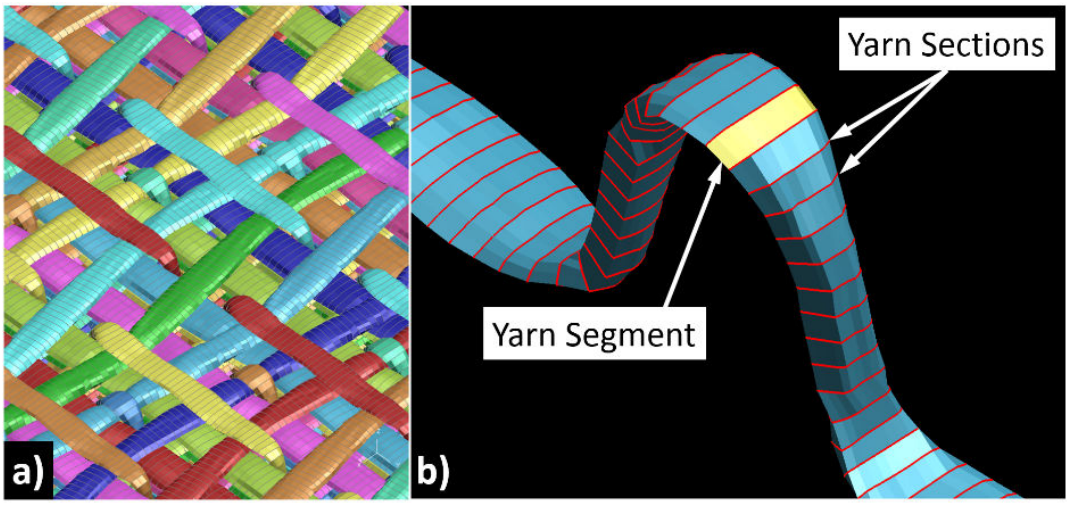

Figure 3. Fabric yarn architecture. a) Model of the full fabric of a 3D orthogonal 5 harness satin weave, b) Yarn geometry definitions showing yarn segments and sections.

4 –High Fidelity Models of 3D Woven Composites

4.1 - Micro Mechanical Models

Mechanical properties for this level are combined from both micro-scale material models and the yarn architectures. A key input to the micro-scale models is the IYVF calculated from the meso-level geometry. For each yarn segment as defined in Figure [3], the IYVF can be calculated directly from the kinematic model outputs. For each yarn segment, a 3D Delunay triangulation is built using the points forming the start and end sections. The volume enclosed within each section can then be triangulated and compared to the volume of fibres used to weave the yarn. This information is then fed into a micro-scale mechanical model where the equivalent yarn properties can be calculated. For this work the analytical model proposed by Chamis [56] is used to calculate an equivalent 3D orthotropic material property for each segment. Figure [4a] shows the variation of intra-yarn volume fraction for the binder yarn in a 3D fabric. The IYVF can be seen to vary as the yarn interacts with other yarns and consequently the material properties change along the yarn length. The other key piece of information to be extracted is the material axes definition which can be obtained from the yarn paths. The material axes for each segment are calculated as the tangent to the yarn centreline at the section seen in Figure [4b]. All triangulations, polyhedra and geometric search trees used in this work are built using the CGAL library [57].

4.2 - Meso Mechanical Models

Once the equivalent 3D orthotropic material properties have been found for every yarn, the next step is to build a finite element mesh to represent the domain of the problem. Several meshing techniques have been proposed to mesh 3D woven composites. However, most of these techniques focus on idealized geometries. Realistic 3D woven geometries with yarn crimp, waviness offer a challenge to such techniques [58], especially if the geometry may contain interpenetrations. Voxel meshes provide a robust alternative for representing the domain complexities. Unlike conventional techniques, for Voxel meshes the domain is meshed in uniform cubes, then each cube is assigned a set of material properties based on its location with respect to the yarn architecture. For the purpose of this work a dedicated multi-scale finite element solver has been developed. This solver uses first order hexahedral elements with 8 integration points. The equivalent orthotropic material properties calculated for each yarn segment is assigned to the integration points located within the yarn surface. The points are located using the same yarn surface 3D triangulations used for calculating IYVF. During element's integration, the micro model is used to correct the material properties based on the intra-volume fraction. Elements with a mix of integration points from inside and outside the yarn are homogenised using an average IYVF across all integration points. Once all the yarns have been mapped, the remaining Voxels are

assigned homogeneous matrix material properties. This model construction approach lends itself to parallelization based on mapping multiple yarns at the same time. Thus greatly enhancing the computational efficiency of the process. The finished model can be solved under any combination of loads and boundary conditions to get a high fidelity prediction of the stresses and strains across the model, which serves as a basis for damage modelling. The solver used in this work uses the PETSC iterative sparse matrix solver package [59, 60] to solve the finite element equations.

4.3 - Voxel meshing of 3D woven composites

Voxel meshing is a robust meshing technique that have seen wide use in FE modelling of woven composites [61-63]. A key strength of Voxel meshes besides the ability to mesh complex geometries, is that these meshes are suitable for Boolean operations. For meshes with similar Voxel size, mesh union and subtraction operations are straight forward. Regions that needs to be removed from a Voxel mesh can be identified by comparison against a triangulation of this region in a similar manner to what was described for the properties mapping. Mesh union can be done by simply adding the Voxel from two or more meshes together then running node equivalence. In addition to unions and subtractions, geometric boundaries can be applied to Voxel meshes, which works in a similar fashion to subtraction but instead of removing the elements and nodes located inside a given region, the process retains the nodes and elements within the region of interest and removes the rest of the elements. Using these tools any geometry, regardless how complex, can be modelled using a combination of Boolean operations as shown in Figure [5].

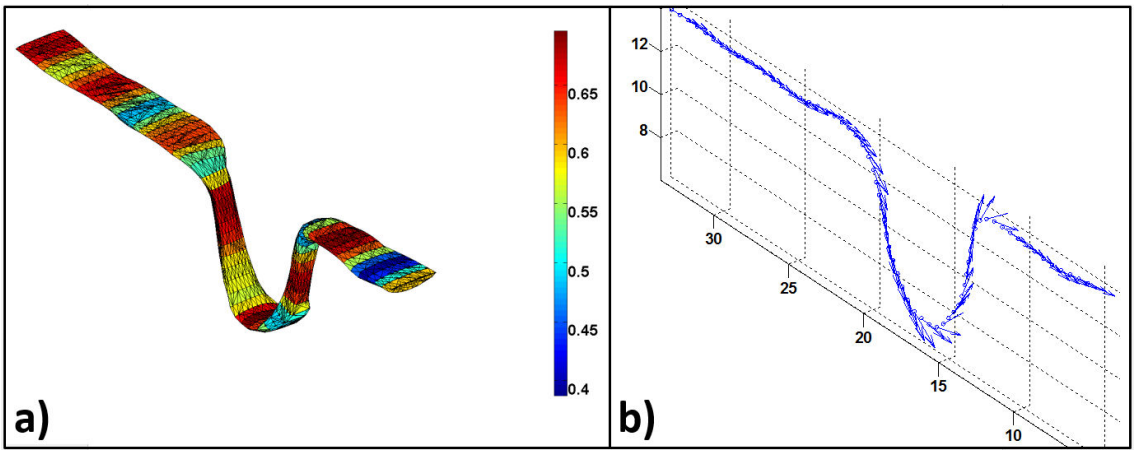

Figure 4. a) As-woven yarn surface triangulation showing IYVF. b) Material axis mapping

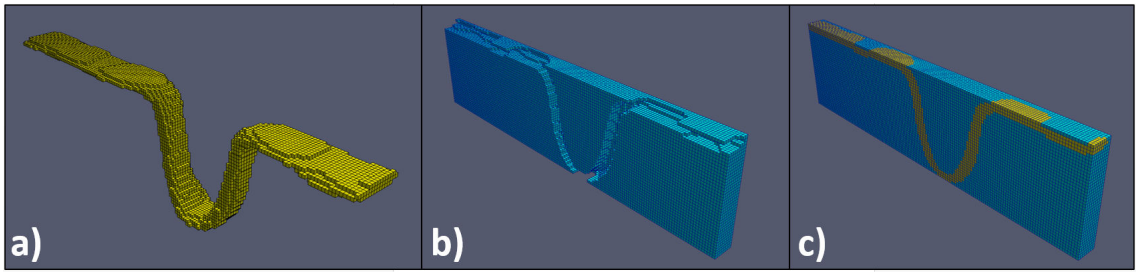

Figure 5. Boolean operations for Voxel meshes; a) boundary application, b) subtraction, c) union.

Figure [6] shows the pseudo-code for an automated material mapping process to generate 3D woven mechanical models from geometric fabric definitions. The material properties used for meso models are shown in Table [1]. The properties of the constituents used to construct the model are given by Green et al [58] for the same materials. The material mapping results and the IYVF results for a preform compacted to 57% VF are shown in Figure [7]. The axial and transverse stresses predicted by this model are shown in Figure [8].

Subroutine *Material Mapping*

1. For each yarn
    I. For each cross-section
        1. Build segment surface triangulation.
        2. Calculate IYVF.
        3. Calculate 3D orthotropic material properties.
        4. Define rotation matrices.
2. For each Voxel element
    I. For each quadrature point
        1. Locate quadrature point w.r.t segment triangulation.
        2. If point is locate inside yarn surface assign material properties and rotation matrices
3. For each Voxel element
    I. For each unassigned quadrature point
        1. Assign matrix material properties.
4. Submit to mechanical solver.
5. End subroutine

Figure 6. Pseudo-code for 3D woven / Voxel material mapping.

Table 1. Model material properties [58]

	E_{11}(MPa)	$E_{22} = E_{33}$ (MPa)	$G_{12} = G_{13}$ (MPa)	G_{23}(MPa)	$\nu_{12} = \nu_{13}$	ν_{23}
Carbon Fibre	238	13	13	6	0.2	0.25
Matrix (MVR444)	3.1	3.1	1.2	1.2	0.35	0.35

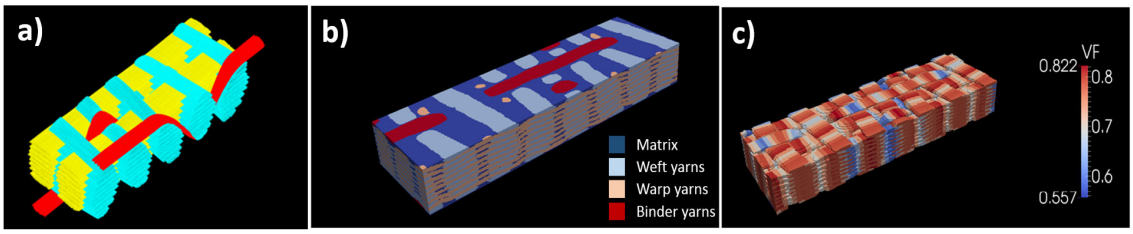

Figure 7. Mapping process result. a) Unit cell geometry b) Material properties assignment, c) Intra-yarn volume fraction distribution (only yarn Voxels shown).

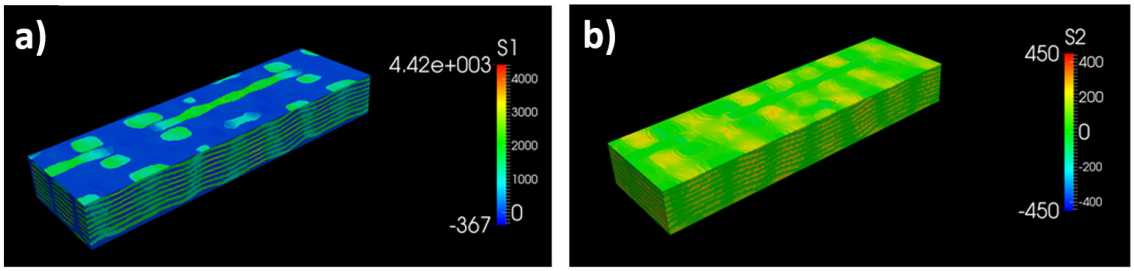

Figure 8. FE analysis results showing stress distribution on a 3D woven composite samples loaded in tension along the warp direction, a) Global stresses along the loading axis, b) Global stresses perpendicular to the loading axis.

5 - Full scale models using spatial Voronoi tessellation

The meso-model described in the previous section is not practical from a computational expense point of view to apply to the feature or structural scale. In order to accurately describe the yarn surface geometries and resin pockets, a high fidelity mesh with a large number of elements is required. To avoid this cost we propose a macro scale modelling approach using a Voronoi tessellation as a basis for homogenization. Voronoi tessellation is a numerical algorithm to divide a spatial domain into completely interlocking cells which tessellate to form the original domain. The conventional tessellation creates its cells such that for all the points inside a cell with a given centre, the distance to the cell centre is smaller than the distance to any other centre in the given domain. Voronoi tessellation has been used in multi-scale modelling of heterogeneous materials with cells built around the heterogeneities as geometric centres [64-66]. Each Voronoi cell is then homogenised taking into account the heterogeneity in the centre. Several challenges face applying the conventional Voronoi tessellation to the 3D composites. First, the yarns follow complex paths which may or may not be related to a specific layer. Additionally, the yarn cross-section changes for each yarn segment. Hence, it is required to expand the tessellation to account for the 3D nature of the problem and for the variability of the yarn cross-section.

For this work, the conventional 2D point based tessellation has been replaced by a 3D volume based tessellation. In this tessellation, the yarn segment surfaces have been used as tessellation generators. As a result, the cells are the volumes closest to a given segment of a yarn surface. Since each yarn segment is straight, the typical Voronoi cell consists of a single straight yarn segment surrounded by an arbitrary region of matrix material. The precise shape of the cell outer surface is dependent on the yarn segment cross-section shape and also the yarn segments geometry in its vicinity and is generally irregular. Consequently, the tessellation decomposes the 3D composite structure into a set of interlocking cells each containing a 1D yarn segment. Each cell material properties can be homogenized using volume integration over a very fine grid to calculate the cell homogenized material properties with no need for orientation averaging. The averaged material properties are considered to be acting in same direction as the 1D yarn segment at its centre. These 3D orthotropic material properties are then assigned to a macro voxel mesh of the complete structure. The result of the complete process is that the structure has been divided into a set of completely interlocking Voronoi cells which fill the complete domain. Thus, an intermediate length scale to replace the yarn/layer length scale has been created. At this scale, the loads and boundary conditions can be applied and the displacements fields calculated. Since the yarn directions have been maintained in the macro-scale model, the displacement field is expected to show a level of heterogeneous behaviour which will prove beneficial when solving the meso-scale boundary value problem.

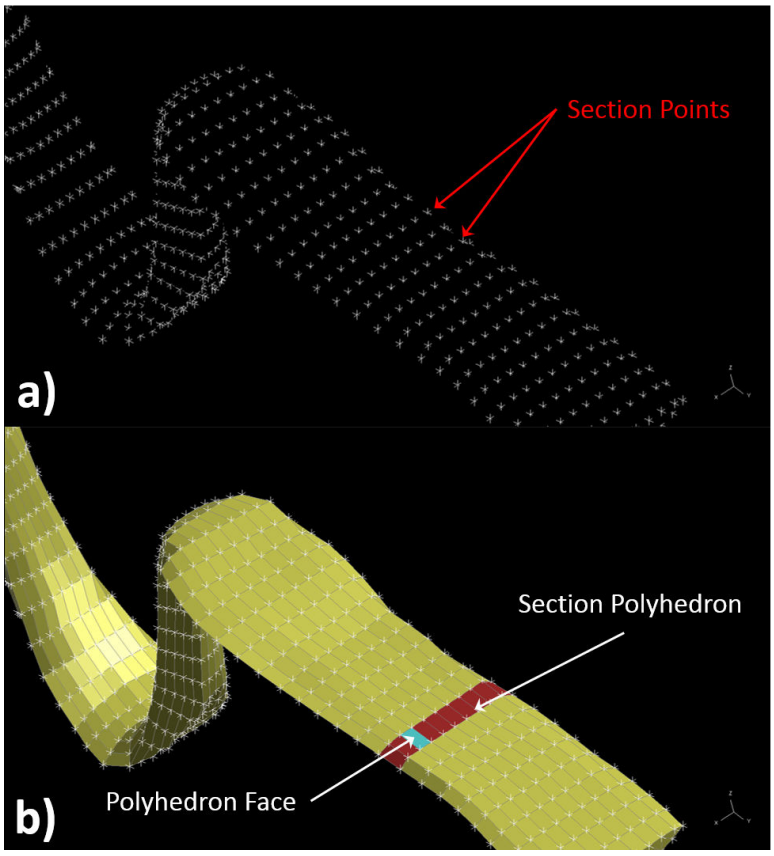

Figure 9. Voronoi tessellation generators a) Yarn segment defined by points b) Yarn segments represented as polyhedron.

For the homogenization to be successful it is essential to have a Voronoi tessellation which satisfies two conditions:

- The tessellations cover the complete domain with no regions left without being assigned to a Voronoi cell.
- The Voronoi cells are mutually exclusive which ensures that there is no overlap of the cells to avoid inaccurate homogenization.

Figure [9.a] shows the yarn section points extracted from the geometric modelling phase for an example yarn. Figure [9.b] shows the results of a yarn surface generated by applying a convex hull to each group of section points. A polyhedron can be generated from the section convex hull to represent the yarn surface at this location. Each polyhedron is closed and built from a set of planar faces. In a Euclidean space $\boldsymbol{S}$ given a set of tessellation generators A, representing the yarn segments is defined as:

$$A = \{A_1, A_2, \dots, A_n\} \ , 2 \leq n < \infty$$

The generators in the proposed tessellation are the polyhedra representing the yarn surface segments. Thus A_i for a given yarn segment is defined by:

$$A_i = \{f_{i1}, f_{i2}, \dots, f_{im}\}, 3 \leq m < \infty$$

Where f_{ij} is the j^{th} face of the i^{th} yarn segment. For all the points p in $\boldsymbol{S}$ we define a Voronoi mapping function $g(p,A_i)$. Where g is defined as:

$$g(p, A_i) = \begin{cases} 1, & if \ \|d_i\| \leq \|d_j\| \\ 0, & otherwise \end{cases}$$

Where d_i and d_j is the distance between the point p and the i^{th} and j^{th} polyhedron calculated as the distance from the nearest face f_{im} in A_i. Okabe et al [67] defines two conditions for the cells of a generalized Voronoi tessellation to be collectively exhaustive and mutually exclusive. The first condition given as:

$$\sum_{i=1}^{n} g(p, A_i) \geq 1, \quad p \in \boldsymbol{S}$$

This condition indicates that all the points in $\boldsymbol{S}$ are assigned to at least one Voronoi cell. For the proposed tessellation, this conditions is satisfied by the proposed mapping function since each point is assigned to at least one cell which contains the closest face. The second condition concerns the boundary of any two adjacent Voronoi cell $V(A_i)$ and $V(A_j)$ which is defined by the set of points $b(A_i, A_j)$ given by:

$$b(A_i, A_j) = \{p | g(p, A_i) = g(p, A_j) = 1, p \in \boldsymbol{S}\}$$

For the exclusivity condition to be satisfied, in a Euclidian space, the set of point $b(A_i, A_j)$ should not have a positive volume. For the case of using the yarn segments as generators, based on the kinematic modelling constraints, which were used to generate the yarn architecture in the first place, yarns are not allowed to interpenetrate. Moreover, in the case of contacting yarn segments, each segment is defined by it is own set of points. This guarantees that the following conditions is universally true for the fabric:

$$A_i \cap A_j = \emptyset, i \neq j$$

This relation guarantees that the boundary of any two Voronoi cells will be open and will not have a positive volume. Thus it is guaranteed that the Voronoi cells will be both exhaustive and mutually exclusive.

Subroutine *Voronoi Homogenization*

1. Call subroutine *Build Search Tree.*
2. Build homogenization High Definition (HD) grid.
3. Do material mapping on HD grid.
4. For each grid point
   I. Search Tree for nearest yarn section.
   II. Add grid point to yarn-section Voronoi cell.
5. Do volume integration over HD grid.
6. Build Macro-scale mesh.
7. For each Macro-scale element
   I. Search Tree for nearest Voronoi Cell.
   II. Assign Voronoi Cell Material properties to element.
8. Submit macro-mesh to FE solver.

Subroutine *Build Search Tree*

1. For each yarn
   I. For each cross-section
      1. Build cross-section convex hull.
      2. Convert convex-hull to a polyhedron.
      3. Extract faces from polyhedron.
      4. Add all faces to Search Tree.
   II. Link faces to cross-section IYVF and axis.
2. End subroutine

Figure 10. Pseudo-code for Voronoi homogenization.

Using the proposed tessellation, a problem domain containing any 3D yarn architecture can be completely divided into cells which serves as basis for homogenization. The pseudo-code for the implementation of this homogenization algorithm is shown in Figure [10]. The core of this homogenization algorithm is organizing the faces defining each yarn surface into a search tree. The search tree is used to calculate the homogenized properties and to assign these properties to the macro-scale Voxel mesh. The search trees in this work was implemented using the AABB Tree from the CGAL library. Figure 11. shows the tessellation process applied to a simple reinforcement geometry. The geometry shown here is of two out of phase spiral yarns embedded in a cuboidal domain. The tessellation decomposes the domain into a set of interlocking cells which are assigned to specific yarn sections. Multiple cross-section are taken along the domain length to show how the domain is divided between the two yarns. The same approach used to decompose the two yarns problem in Figure 11 can be used to decompose any 3D woven composite, regardless of its complexity or the number of yarns.

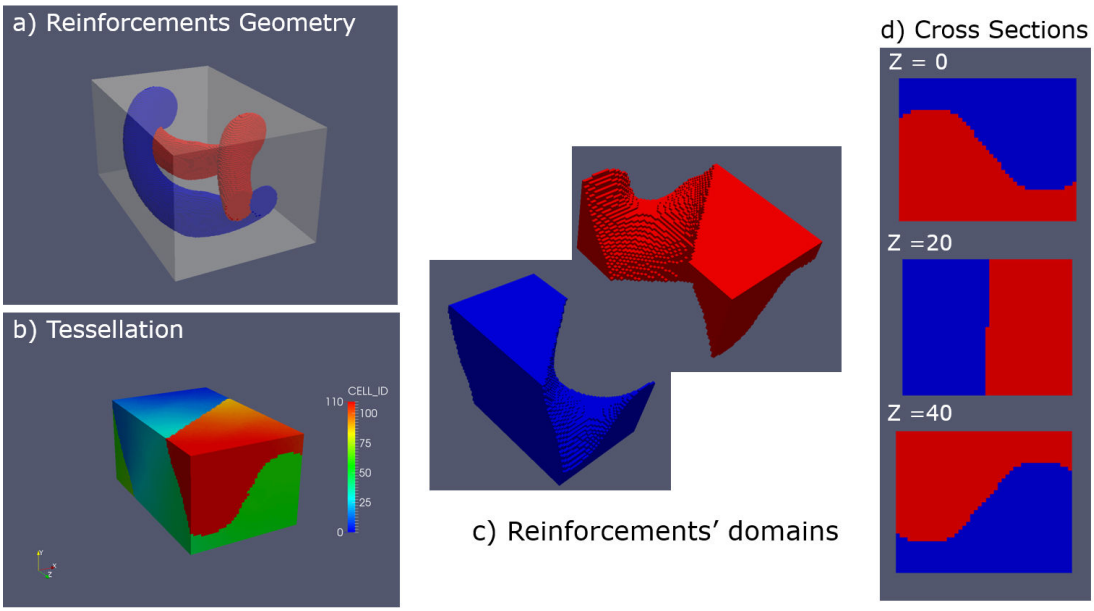

Figure 11. 3D spatial Voronoi tessellation applied to a simple geometry, a) Reinforcements geometry, b) Domain decomposition using Voronoi tessellation, c) Reinforcements' domains after decomposition, d) Cross-sections across the tessellation domain.

For purpose of model verification and validation, a set of meso and macro models have been created and compared against experimental results. Three sets of models have been solved where each set models a specific physical experiment. The models include two tensile samples, one loaded in the warp direction and the other in the weft direction, and a V-notch rail shear test [68]. The high fidelity models, loading directions and the Voronoi models are shown in Figure [12]. For the shear test, the shear modulus was calculated following the ASTM standard D 7078 which uses the cross-section area between the two notches to calculate modulus. The same standard was applied to calculate the shear modulus from the meso and macro scale models. The elastic moduli predicted by both the meso and the macro scales have been compared against the value measured by experiments. The results are shown in Table [2]. Model sizes data are shown in Table [3]. The elastic response is shown to be in good agreement for the two model types with the experimental results for all three load cases. For 2D composites, the transverse direction properties of the fibres is a usual source of modelling uncertainty. In contrast, for 3D woven composites, fibres are present in all three main directions. Hence, the response is controlled by the fibre axial properties and the transverse properties have minimal effect on the stiffness response. Consequently, the elastic response can be predicted accurately if the internal yarn architecture is considered in detail.

The weft loaded samples were compared against stereo Digital Image Correlation (DIC) measurements for a similar physical sample. The model took into consideration the exact specimen yarn architecture in relation to the specimen boundary. This was done to include edge effects present in the experiment in the models. The full width of the specimen and 4 unit cells in the gauge direction with periodic

boundary conditions was modelled. The model was displacement controlled and loaded to the same level as the experiment. The results were compared in terms of the in-plane transverse displacement and out of plane transverse displacement. The axial strain response is dominated by the applied displacement. Hence, the comparison in the axial direction does not yield any additional knowledge of the sample behaviour. The comparisons are shown in Figure [13] and Figure [14]. Both the macro and meso models have captured the in-plane transverse displacement with good accuracy. For, the out of plane displacement both models were capable of capturing the hotspots in the experiment which correspond to the binder yarn locations. The surface strain profiles along path "A" from Figure [13] have been plotted in Figure [15]. The macro and meso model capture the general trend present in the DIC results. Additionally, the strain profiles shown in Figure [15] show a strong variation across the specimen. This can be explained by the presence of strong interaction between the internal yarn architecture and the sample size.

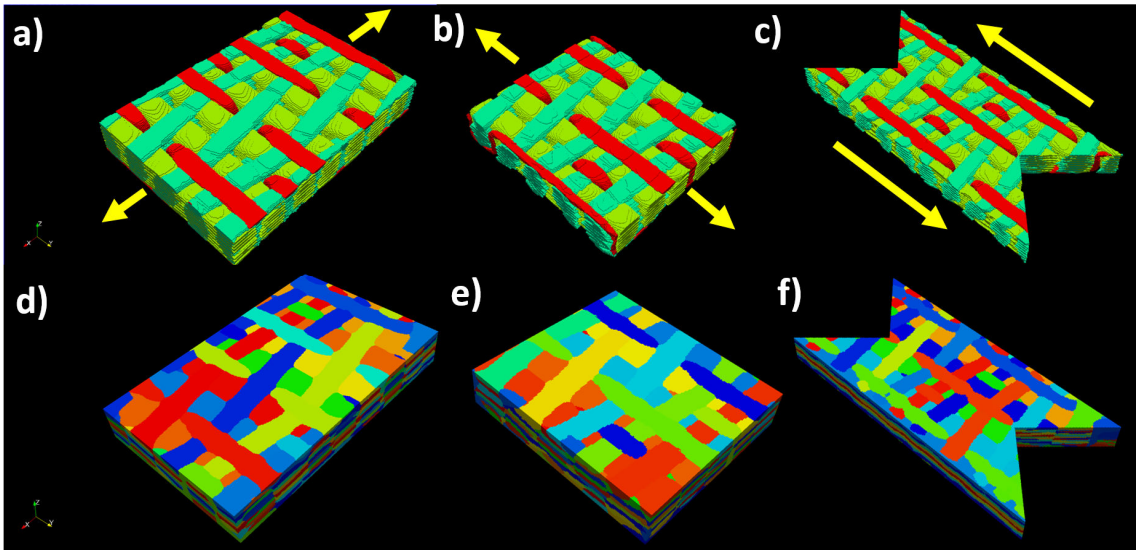

Figure 12. Models used to calculate 3D woven composite elastic constants, a) High fidelity weft direction (showing only yarn elements), b) High fidelity warp direction, c) High fidelity shear specimen, d) Homogenized weft direction, e) Homogenized warp direction, f) Homogenized shear specimen

Table 2. The elastic moduli predicted by the macro and meso models in comparison to the experimental results.

	Experimental (GPa)	**Meso-Scale (GPa)**	**Macro-Scale (GPa)**
Young's modulus warp	63.9	64.0	63.0
Young's modulus weft	60.8	61.0	60.0
In-plane shear modulus	4.7	4.8	4.3

Table 3. Model size comparison for macro and meso models.

	E_x – Meso (Warp)	E_x – Macro (Warp)	E_y–Meso (Weft)	E_y-Macro (Weft)	G_{xy}-Meso (Shear)	G_{xy}-Macro (Shear)
Model size in million degrees of freedom	15	0.94	15	0.94	30	1.875

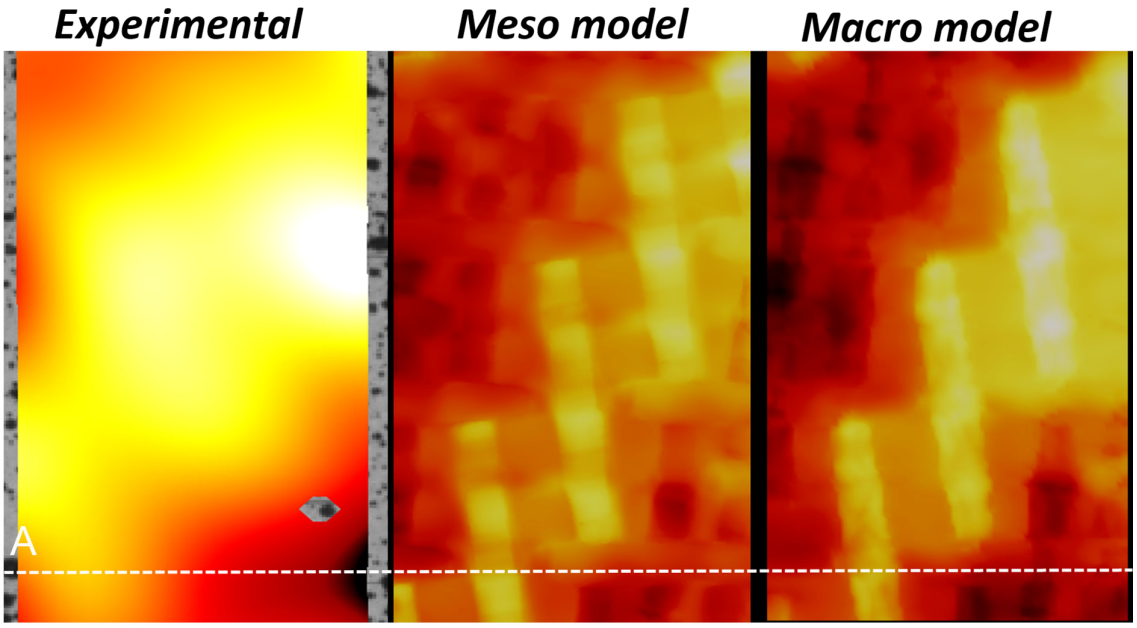

Figure 13. A comparison of the in-plane transverse strain from weft loaded specimens; DIC and FE models (loading in the vertical direction).

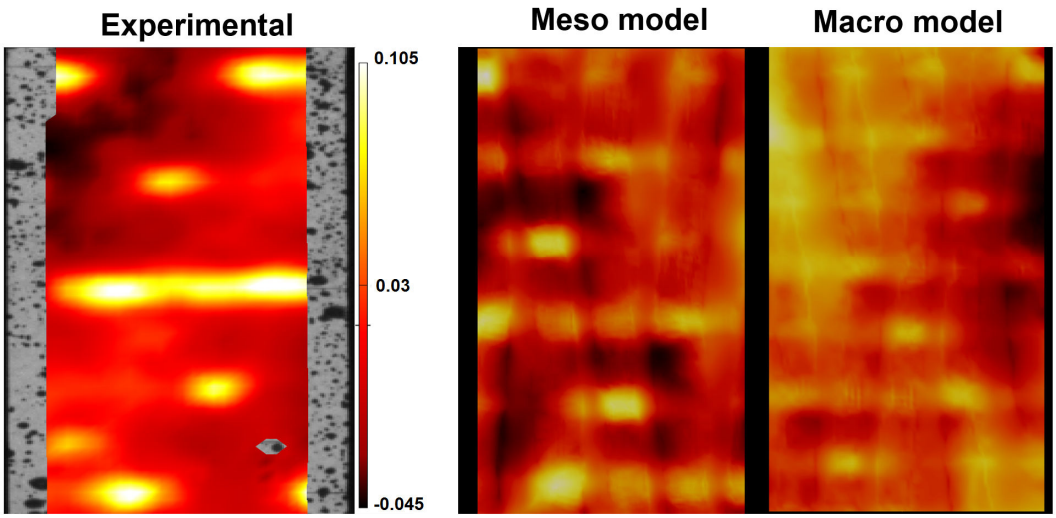

Figure 14. A comparison of the out of plane displacement from weft loaded specimens; DIC and FE models (loading in the vertical direction).

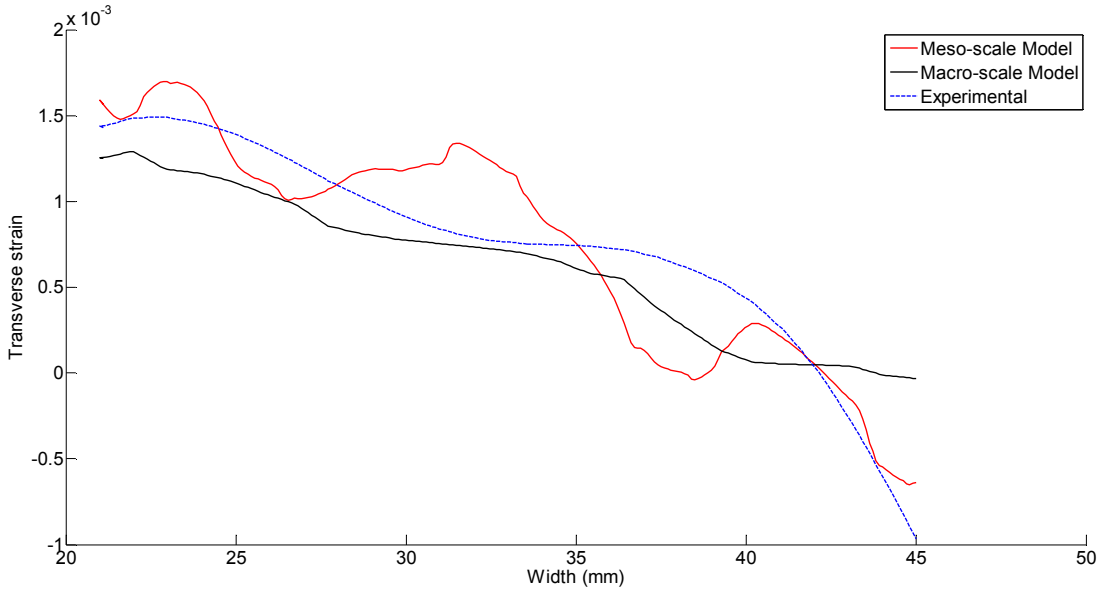

Figure 15. Comparison of transverse surface strain profiles between meso, macro and experimental DIC

For the V-notch shear test, the critical section is the through thickness slice at the middle of the specimen where the sample is narrowest. The in-plane shear strain acting on the middle slice as calculated by both the macro and meso models is shown in Figure [16]. A comparison of the mid-plane strain along on the same sections is shown in Figure [17]. It can be seen that the average strain and the general loading trend is in agreement in both models. On the other hand, the concentrations resulting from the geometry

details have been lost in the homogenised macro approach. As stated in section 1, it is important to include the effects of the meso level stress concentrations in mechanical modelling since these features drive the damage initiation, leading to ultimate failure of the composite. An additional step is needed to complete the multi-scale modelling approach by introducing a coupled global-local analysis for the highly loaded regions.

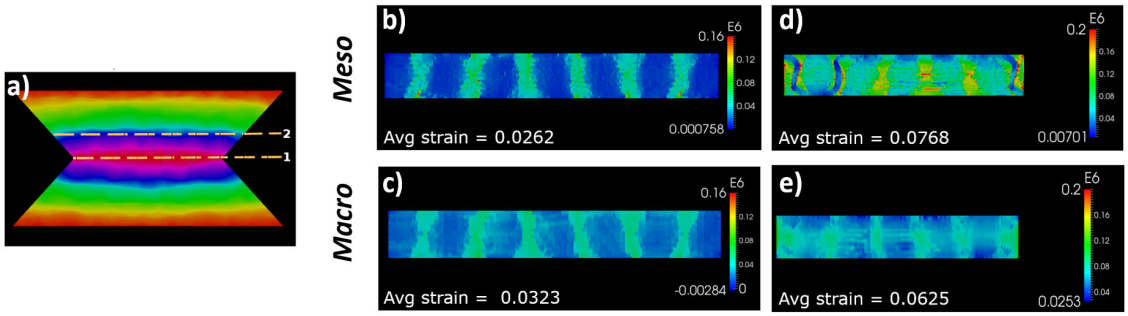

Figure 16. Through thickness sections showing In-plane shears train comparisson between macro and meso model at two different locations within V-notch shear sample. a) Contour of displacment maginitude on a the sample. b) Meso model inplane shear strain on section 1. c) Macro model inplane shear strain on section 1. d) Meso model inplane shear strain on section 2. e) Macro model inplane shear strain on section 2.

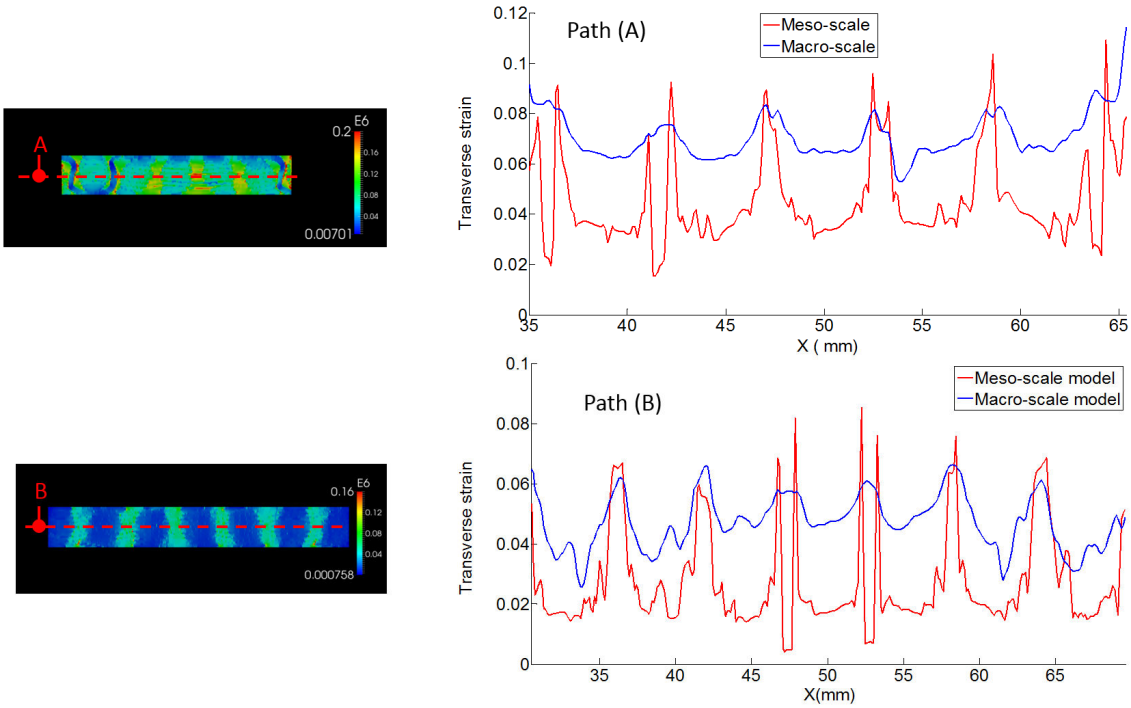

Figure 17. A comparison of the strain calculated by the meso and macro models on sections 1 and 2 from Figure [16].

6- Meso-scale boundary value problems

Once the macro-scale problem has been solved and the displacement field calculated, the highly loaded regions within that model can be determined with reasonable accuracy. At this stage the overall stiffness of the component has been calculated and the next stage of analysis is to understand the failure envelope of the structure under investigation. A detailed meso-scale model can be built based on the internal yarn architecture as shown in section 4. This meso scale model can be solved as a boundary value problem under boundary conditions extracted from the macro model. This is done by creating a set of Lagrangian Multipliers acting on the meso-model. These Lagrangian Multipliers represent the boundary displacement of the meso-scale, described in terms of macro-scale displacement in form:

$$u_m = \boldsymbol{N} u_M \tag{1}$$

Here $\boldsymbol{N}$ is the coefficient matrix of the Lagrangian multipliers equations, u_m is the meso scale boundary displacement, u_M is the macro model displacement. To ensure a smooth transition between the macro and meso-scales, the macro element shape functions are used to compile the Lagrangian equations. Initially, a critical region is located from the macro-model and then a new high fidelity model is built for this region which uses direct material properties mapping with no homogenization. A convex hull is then constructed over the meso mesh nodes. The nodes that form the convex hull are the meso mesh boundary nodes, which need to be constrained by the Lagrangian multipliers. The nodal coordinates are then converted from the meso model axis to the macro model axis and to the nearest macro element intrinsic coordinates. The macro element shape function is then used to interpolate the meso node displacement in terms of macro element nodal displacements which are assembled into the coefficient matrix $\boldsymbol{N}$. The Lagrangian equations are then added to the set of finite element equations generated by the meso-scale model giving:

$$\begin{bmatrix} K_m & N^T \\ N & 0 \end{bmatrix} \begin{bmatrix} u_m \\ \lambda \end{bmatrix} = \begin{bmatrix} f_m \\ 0 \end{bmatrix} \tag{2}$$

Where K_m is the stiffness matrix of the meso-scale model and λ is the Lagrangian multiplier forces. Lagrangian multipliers by definition introduce singularities to the diagonal of the system matrix, which in turn causes most linear equations solvers to fail. As a result, the complete system has to be solved in an iterative process where the Lagrangian multiplier forces are fed back to the macro-scale system. The Lagrangian forces can be projected on the macro-scale mesh using the Moore-Penrose pseudoinverse of the coefficient matrix N^+ after scaling for macro/meso mesh size ratio. In this approach, the macro-scale degrees of freedom can be divided into internal and boundary degrees of freedom following the FETI approach [19, 69]. Then the macro system can be rewritten as:

$$\begin{bmatrix} K_M^{ii} & K_M^{ib} \\ K_M^{bi} & K_M^{bb} \end{bmatrix} \begin{bmatrix} u_M^i \\ u_M^b \end{bmatrix} = \begin{bmatrix} f_M^i \\ f_M^b - N^+ \lambda \end{bmatrix} \quad (3)$$

Here, K_M^{ii} is the stiffness matrix of the internal degrees of freedom. K_M^{bb} is the stiffness matrix components associated with the degrees of freedom on the boundary between the meso and macro models. K_M^{bi} and K_M^{ib} is the macro stiffness boundary/internal coupling terms. u_M^i is the displacement associated with the internal degrees of freedom on the macro-scale. u_M^b is the displacement associated with the boundary degrees of freedom. f_M^i is applied forces associated with the macro-scale internal degrees of freedom and f_M^b is applied forces associated with meso/macro boundary. Once the system is setup in this manner, the macro-scale displacements are recalculated under the Lagrangian forces. Then, a new set of meso boundary conditions is calculated. A new meso-scale solution is then found and the iteration process proceeds until convergence. The solution convergence speed in the proposed approach is greatly enhanced by using the full macro model solution as an initial condition for the iteration process. In this manner, the global/local analysis is concerned with finding the difference between the homogenized and high fidelity solutions rather than solving the complete problem. Also, it is worth noting that for the model sizes in this paper where the models have tens of millions of degrees of freedom, sparse matrices and iterative solvers are the only practical option for handling this problem. Hence, the problem formulation had to be adapted accordingly.

The V-notch shear specimen used in the previous section to predict the in-plane shear modulus of the fabric being studied is a good example where a hybrid multi-scale model can be used. The critical region of this sample is in the middle, where the sample is narrowest and the average strain is highest. The multi-scale model was applied to this type of test and the results compared to a full meso-model of the specimen. The result for the strain field and the overall displacement are shown in Figure [18] and Figure [19]. The comparison shows that there is no detectable displacement discontinuity between the macro and meso regions in the hybrid model. A key drawback of many global-local analysis approaches is the presence of discontinuities between the global and local scales. These discontinuities can lead to stress artefacts in the meso-models. For the proposed modelling approach, since the macro displacement field is heterogeneous and follows the same pattern as the meso scale, no such stress artefacts can be seen in the meso model. Figure [20] shows displacement field on the interface between the meso and macro scale (u_M^b) which has been calculated by solving equations [2] and [3] simultaneously. Figure [21] shows the stress distribution on the middle slice as predicted by both the multi-scale and the full meso scale model. Figure [22] shows a comparison of the strain profiles on a path across the sample between the hybrid and meso-scale model. It can be seen that the two models are in good agreement an there is no significant strain discontinuities along this path. The multi-scale model solves the same problem with 2.5 million degrees of freedom as compared to 30 million for the full meso scale solution.

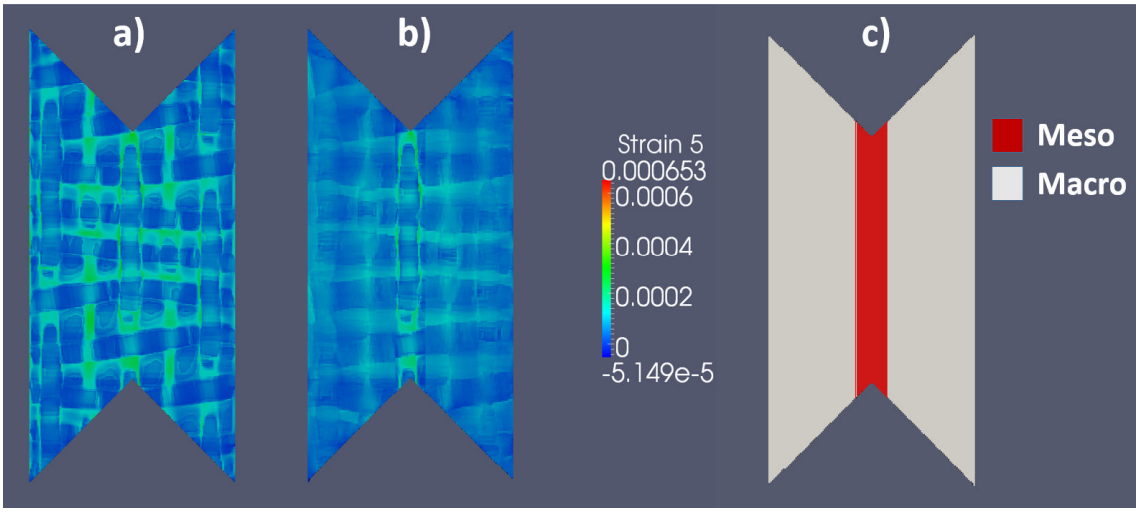

Figure 18. A comparison of in plane shear strain for a V-notch test. a) Full meso scale model b) Hybrid meso/macro model. c) Hybrid model domain decomposition.

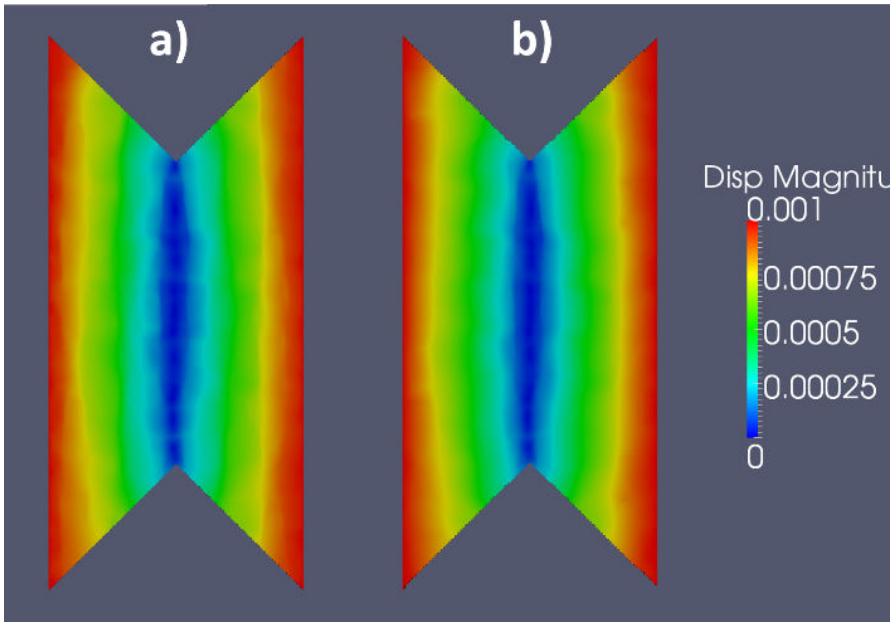

Figure 19. A comparison of total displacement field for a V-notch test. a) Full meso scale model b) Hybrid meso/macro model.

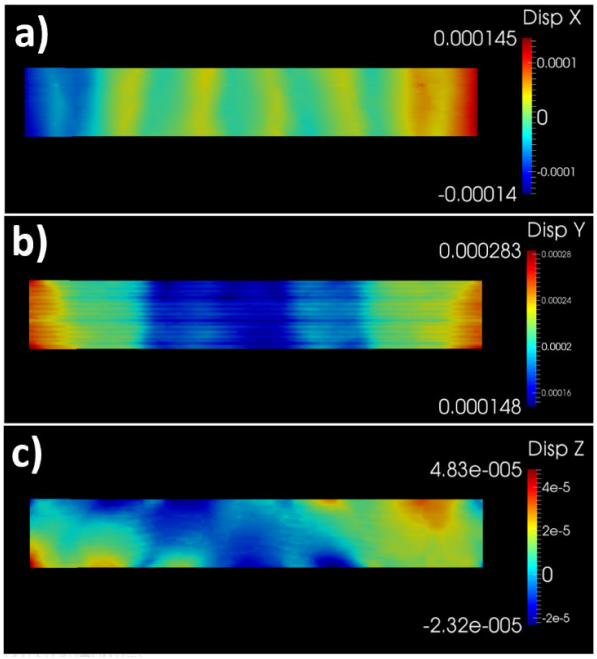

Figure 20. The displacement boundary conditions on the meso-scale model as interpolated from the macro model for the V-notch rail test. a) X displacement (in-plane transverse direction), b) Y displacement (in-plane loading direction), and c) Z displacement (out of plane direction).

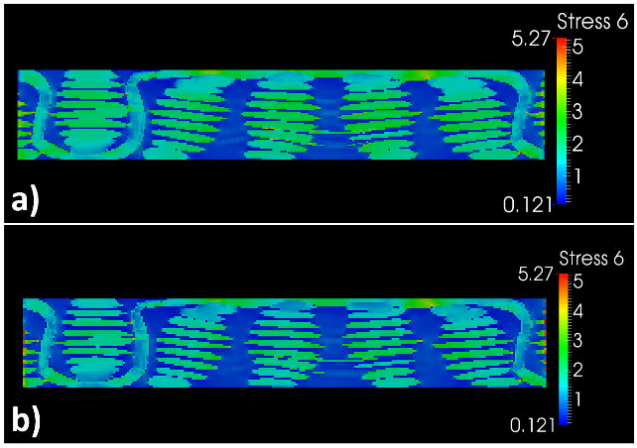

Figure 21. Comparison of in plane shear stress on the middle slice of the V-notch sample. a) Multi-scale model, b) Full meso-scale model

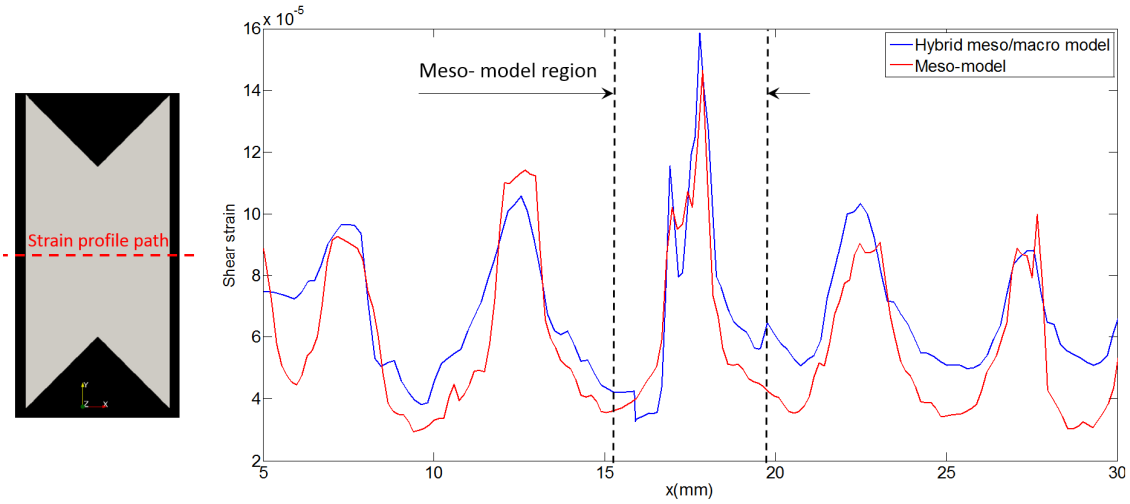

Figure 22. A comparison of the mid-plane strain profile across the V-notch specimen as calculated by the high fidelity model and the hybrid multi-scale model.

An additional strength of the proposed modelling approach is the ability to handle components with complex geometries. The examples studied so far were all sections of flat plates. These samples show edge effects and thus demonstrate the need for multi-scale modelling for even the simplest components. They have not however shown how the proposed model can handle complex geometries. An example of a more complex component geometry is shown in Figure [23]. The geometry has a double curvature with a varying radius at its apex. A kinematic simulation was run to model the deformation and compaction of the orthogonal 3D woven material studied in this work on the tools shown. The kinematic model used to generate this internal yarn architecture for this component is detailed by El Said et al [8]. The internal yarn architecture resulting from the kinematic model is shown in Figure [23 c]. It can be seen that the yarn architecture varies throughout the component as a result of the tool geometry and the initial yarn architecture. The weft yarns on the surface have different levels of waviness between the component apex, the component corners and the flat sections. The section showing the highest level of yarn waviness has been modelled using the proposed multi-scale approach. Figure [24a] shows the homogenised Voronoi model of this section. The model is loaded in compression in the y-axis direction to induce bending stresses in the middle part of the component. The average transverse stress in each yarn as calculated by the macro-scale model is shown in Figure [24b]. Figure [25] shows the multi-scale mesh and the displacement as calculated by the multi-scale model. The full macro-scale model is 2 million degrees of freedom and the hybrid meso/macro is 3.2 million degrees of freedom. Figure [26] displays the fibre direction stresses in the meso-model. Figure [27] shows the yarn transverse stresses and the matrix maximum principal stresses. It can be seen that the stresses are consistent with the bending behaviour expected at this location. Additionally, the model captures the complex nature of the stress state at this scale as would be expected from the complex yarn architecture. The model shows

that the yarn transverse stress, which is the main driver behind matrix cracking in woven composite, is dependent on the yarn crimp and waviness. The weft yarns with the highest crimp and waviness is displaying high transverse stress as well as high matrix stress in the yarn vicinity. Here, it has to be mentioned that despite the considerable reduction in model size between the full meso-scale and the proposed multi-scale model, the analysis is still relatively large. As has been shown, the proposed model can handle feature scale modelling such as the double curvature geometry presented here. However, for even larger structures applying this approach directly might be computationally prohibitive. A further level of homogenization might thus be required to inform or interact with the hybrid model represented here. Several approximate models are available in literature that can fill this role [70-72].

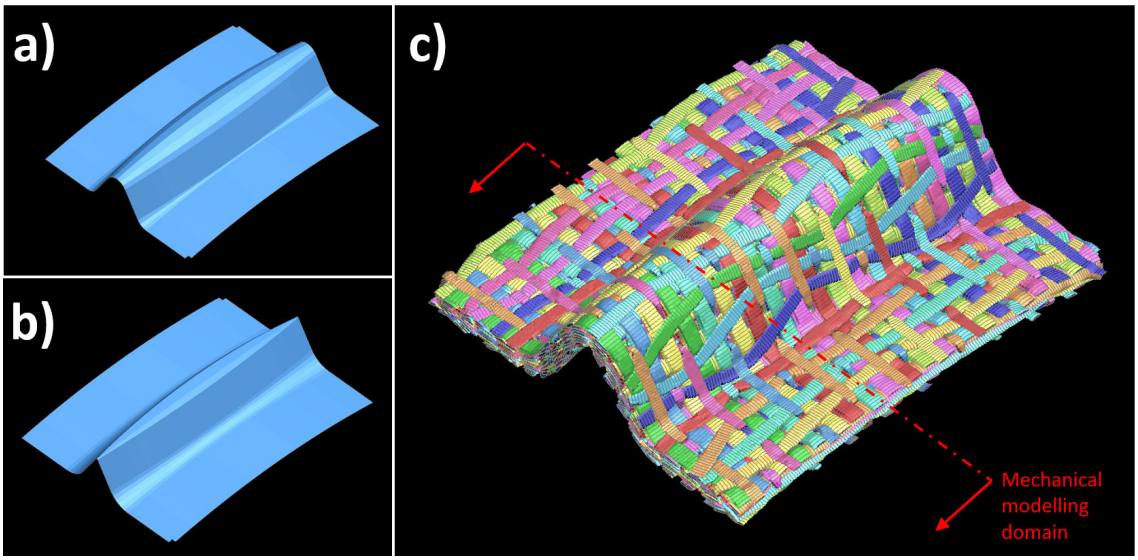

Figure 23. Complex 3D woven component, a) Upper tool surface, b) Lower tool surface, c) Kinematic model of the internal fiber architecture.

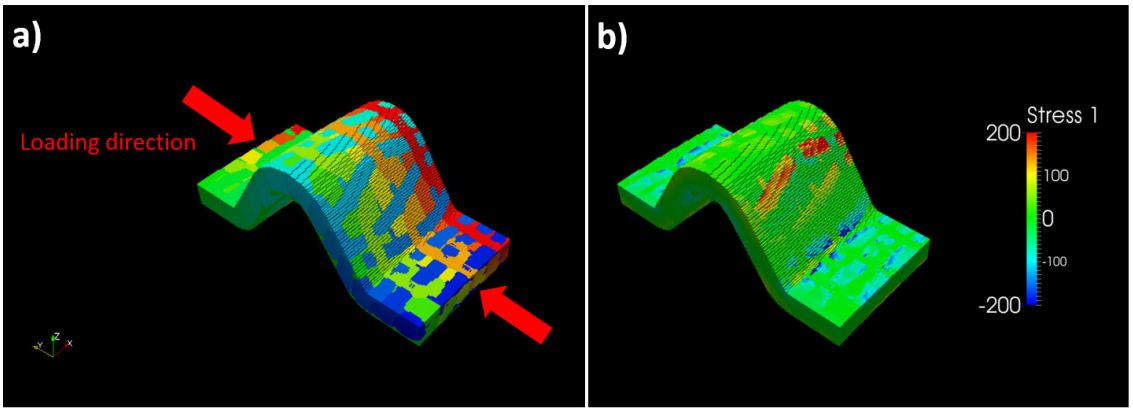

Figure 24. Complex 3D woven component, a) Homogenized Voronoi model b) Yarn transverse stress.

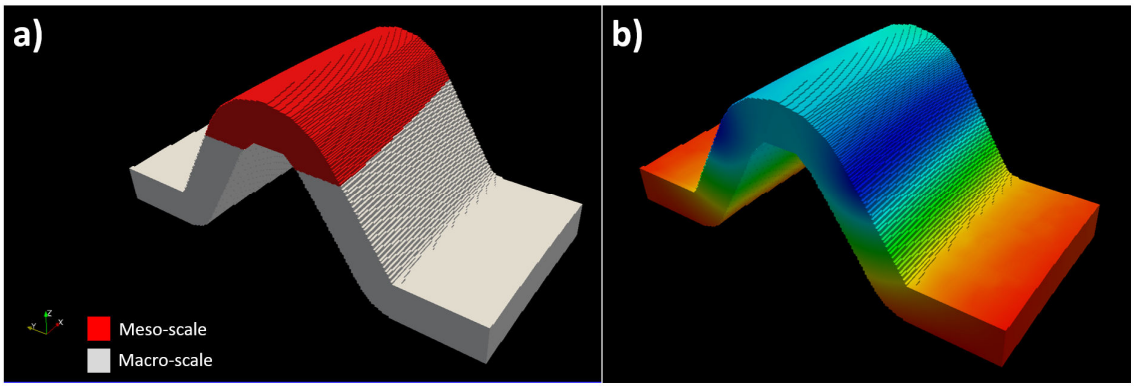

Figure 25. Complex 3D woven component, a) Multi-scale meshes, the red section is the meso and grey is the macro, b) Multi-scale results for displacement magnitude.

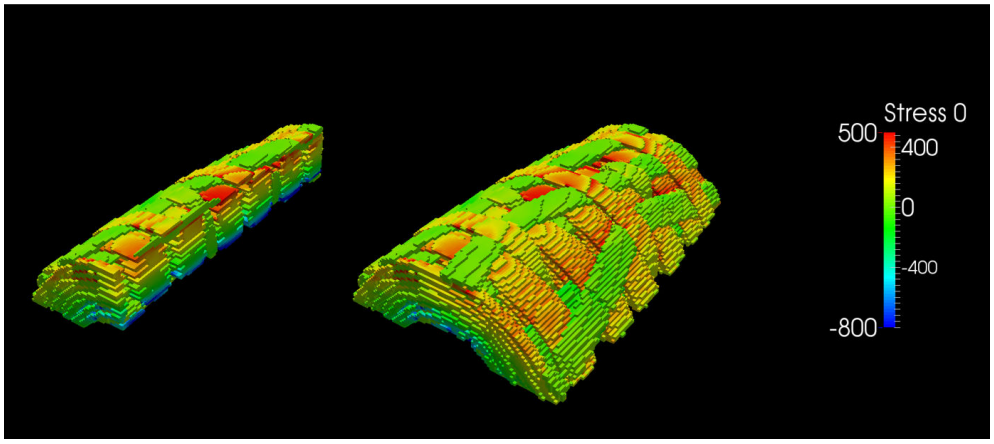

Figure 26. Complex 3D woven component meso model: fiber direction stresses on the full model and a cut section of the same region.

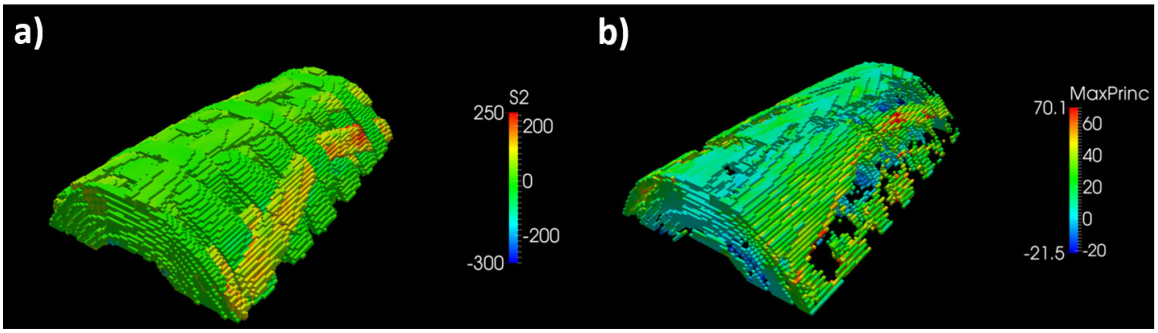

Figure 27. Complex 3D woven component meso model: a) Yarn transverses stresses b) Matrix maximum principal stresses.

7 – Conclusions

In this paper, a novel integrated multi-scale modelling framework for 3D woven structures has been proposed and verified against experimental results. The proposed model has been used to gain insight into the mechanical behaviour of 3D woven composites. The strain and stress distributions found using this modelling approach show a strong relation between the internal yarn architecture and the mechanical response of 3D woven composites. Internal yarn deformations such as crimp and waviness create localized stress concentrations that can act as damage initiators in these structures. Additionally, it has been shown that the internal yarn architecture changes throughout the manufacturing phases and is dependent on the final structural geometry. Consequently, the yarn architecture and the meso-scale mechanical response become no longer only material properties but are also influenced by the specific structure of interest. This observation leads to additional complications when modelling or experimentally testing 3D composites due to the need to consider the yarn architecture at the meso-scale, even for structural scale response.

Composites modelling have traditionally relied on achieving scale separation between the macro and meso scale. Here, it has been shown that for 3D composites the loss of periodicity and the mechanical response dependency on yarn architecture mean that scale separation is no longer feasible. A coupled approach which links the meso-scale to the global structural response is required. This coupled approach needs to include the influence of the internal yarn architecture on both the macro and meso scales. Additionally, coupon testing is a widely used approach of composites characterization. In this work, we have modelled three different specimens commonly used in such tests. The strain profiles calculated by the models show considerable variation throughout the specimens' planform and through thickness. Even for simple test such as a tensile test, the strain distribution shows large variation across the sample width, which is an indicator of strong interaction between the yarn architecture and the sample size. These yarn architecture dependent variations mean that conventional coupon testing of these materials will measure specimen specific properties rather than generic material properties. For 3D woven composite structures with complex geometry, the changes in internal architecture are associated with a changes to the yarn architecture on the meso-scale. As a results, homogenised material properties measured from flat samples or calculated from models of flat samples will not be valid as inputs to structural scale models. This effect has been observed clearly in the double curvature component modelled in this paper. In this model, the highest transverse stresses were observed in regions where the internal yarn architecture showed the highest deformations, as a result of the component geometry. This observation shows that more elaborate specimen design, which is informed by the internal architecture and the final structure geometry, is needed to carry out proper characterisation. The

modelling techniques presented here offer an opportunity to carry out trials of such characterisations in a virtual sense, due to their accurate physical representation of geometry at the relevant scales.

Acknowledgments

The authors would like to acknowledge;

- Rolls-Royce plc for their support of this research through the Composites University Technology Centre at the University of Bristol, UK.
- The Engineering and Physical Sciences Research Council for supporting this work through the Centre for Doctoral Training in Advanced Composites at the University of Bristol, UK (Grant no. EP/G036772/1).
- BAE Systems, Advanced Technology Centre for providing the experimental results used for validation in this work.

References

[1] R. Kamiya, B. A. Cheeseman, P. Popper, and T. W. Chou, "Some recent advances in the fabrication and design of three-dimensional textile preforms: a review," *Composites science and technology,* vol. 60, pp. 33-47, 2000.

[2] A. P. Mouritz, M. K. Bannister, P. J. Falzon, and K. H. Leong, "Review of applications for advanced three-dimensional fibre textile composites," *Composites Part A: Applied Science and Manufacturing,* vol. 30, pp. 1445-1461, 1999.

[3] J. N. Baucom and M. A. Zikry, "Evolution of failure mechanisms in 2D and 3D woven composite systems under quasi-static perforation," *Journal of composite materials,* vol. 37, pp. 1651-1674, 2003.

[4] V. A. Guénon, T. W. Chou, and J. W. Gillespie, "Toughness properties of a three-dimensional carbon-epoxy composite," *Journal of materials science,* vol. 24, pp. 4168-4175, 1989.

[5] J. Brandt, K. Drechsler, and F. J. Arendts, "Mechanical performance of composites based on various three-dimensional woven-fibre preforms," *Composites Science and Technology,* vol. 56, pp. 381-386, 1996.

[6] B. N. Cox, M. S. Dadkhah, W. L. Morris, and J. G. Flintoff, "Failure mechanisms of 3D woven composites in tension, compression, and bending," *Acta metallurgica et materialia,* vol. 42, pp. 3967-3984, 1994.

[7] S. Green, A. Long, B. El Said, and S. Hallett, "Numerical modelling of 3D woven preform deformations," *Composite Structures,* vol. 108, pp. 747-756, 2014.

[8] B. El Said, S. Green, and S. R. Hallett, "Kinematic modelling of 3D woven fabric deformation for structural scale features," *Composites Part A: Applied Science and Manufacturing,* vol. 57, pp. 95-107, 2014.

[9] Y. Mahadik and S. R. Hallett, "Effect of fabric compaction and yarn waviness on 3D woven composite compressive properties," *Composites Part A: Applied Science and Manufacturing,* vol. 42, pp. 1592-1600, 2011.

[10] P. Kanouté, D. Boso, J. Chaboche, and B. Schrefler, "Multiscale methods for composites: a review," *Archives of Computational Methods in Engineering,* vol. 16, pp. 31-75, 2009.

[11] V. Kouznetsova, M. G. Geers, and W. M. Brekelmans, "Multi‐scale constitutive modelling of heterogeneous materials with a gradient‐enhanced computational homogenization scheme," *International Journal for Numerical Methods in Engineering,* vol. 54, pp. 1235-1260, 2002.

[12] M. Kamiński and M. Kleiber, "Numerical homogenization of N‐component composites including stochastic interface defects," *International Journal for Numerical Methods in Engineering,* vol. 47, pp. 1001-1027, 2000.

[13] R. Smit, W. Brekelmans, and H. Meijer, "Prediction of the mechanical behavior of nonlinear heterogeneous systems by multi-level finite element modeling," *Computer Methods in Applied Mechanics and Engineering,* vol. 155, pp. 181-192, 1998.

[14] V. Carvelli and C. Poggi, "A homogenization procedure for the numerical analysis of woven fabric composites," *Composites Part A: Applied Science and Manufacturing,* vol. 32, pp. 1425-1432, 2001.

[15] P. W. Chung and K. K. Tamma, "Woven fabric composites—developments in engineering bounds, homogenization and applications," *International Journal for Numerical Methods in Engineering,* vol. 45, pp. 1757-1790, 1999.

[16] X. Tang and J. D. Whitcomb, "General techniques for exploiting periodicity and symmetries in micromechanics analysis of textile composites," *Journal of composite materials,* vol. 37, pp. 1167-1189, 2003.

[17] Z. Xia, Y. Zhang, and F. Ellyin, "A unified periodical boundary conditions for representative volume elements of composites and applications," *International Journal of Solids and Structures,* vol. 40, pp. 1907-1921, 2003.

[18] R. Hill, "Elastic properties of reinforced solids: some theoretical principles," *Journal of the Mechanics and Physics of Solids,* vol. 11, pp. 357-372, 1963.

[19] C. Farhat and F. X. Roux, "A method of finite element tearing and interconnecting and its parallel solution algorithm," *International Journal for Numerical Methods in Engineering,* vol. 32, pp. 1205-1227, 1991.

[20] C. Farhat and F.-X. Roux, "An unconventional domain decomposition method for an efficient parallel solution of large-scale finite element systems," *SIAM Journal on Scientific and Statistical Computing,* vol. 13, pp. 379-396, 1992.

[21] C. Farhat, M. Lesoinne, P. LeTallec, K. Pierson, and D. Rixen, "FETI‐DP: a dual‐primal unified FETI method−part I: A faster alternative to the two‐level FETI method," *International journal for numerical methods in engineering,* vol. 50, pp. 1523-1544, 2001.

[22] P. Ladevèze, O. Loiseau, and D. Dureisseix, "A micro–macro and parallel computational strategy for highly heterogeneous structures," *International Journal for Numerical Methods in Engineering,* vol. 52, pp. 121-138, 2001.

[23] D. Markovic and A. Ibrahimbegovic, "On micro–macro interface conditions for micro scale based FEM for inelastic behavior of heterogeneous materials," *Computer Methods in Applied Mechanics and Engineering,* vol. 193, pp. 5503-5523, 2004.

[24] P.-A. Guidault, O. Allix, L. Champaney, and C. Cornuault, "A multiscale extended finite element method for crack propagation," *Computer Methods in Applied Mechanics and Engineering,* vol. 197, pp. 381-399, 2008.

[25] A. Puck and H. Schürmann, "Failure analysis of FRP laminates by means of physically based phenomenological models," *Composites Science and Technology,* vol. 58, pp. 1045-1067, 1998.

[26] R. Cuntze and A. Freund, "The predictive capability of failure mode concept-based strength criteria for multidirectional laminates," *Composites Science and Technology,* vol. 64, pp. 343-377, 2004.

[27] R. M. Caddell, R. S. Raghava, and A. G. Atkins, "Pressure dependent yield criteria for polymers," *Materials Science and Engineering,* vol. 13, pp. 113-120, 1974.

[28] S. Pinho, L. Iannucci, and P. Robinson, "Physically based failure models and criteria for laminated fibre-reinforced composites with emphasis on fibre kinking. Part II: FE implementation," *Composites Part A: Applied Science and Manufacturing,* vol. 37, pp. 766-777, 2006.

[29] M. Donadon, L. Iannucci, B. G. Falzon, J. Hodgkinson, and S. F. de Almeida, "A progressive failure model for composite laminates subjected to low velocity impact damage," *Computers & Structures,* vol. 86, pp. 1232-1252, 2008.

[30] M. Vogler, R. Rolfes, and P. Camanho, "Modeling the inelastic deformation and fracture of polymer composites–Part I: plasticity model," *Mechanics of Materials,* vol. 59, pp. 50-64, 2013.

[31] P. Camanho, M. Bessa, G. Catalanotti, M. Vogler, and R. Rolfes, "Modeling the inelastic deformation and fracture of polymer composites–Part II: smeared crack model," *Mechanics of Materials,* vol. 59, pp. 36-49, 2013.

[32] I. Lapczyk and J. A. Hurtado, "Progressive damage modeling in fiber-reinforced materials," *Composites Part A: Applied Science and Manufacturing,* vol. 38, pp. 2333-2341, 2007.

[33] W. G. Jiang, S. R. Hallett, B. G. Green, and M. R. Wisnom, "A concise interface constitutive law for analysis of delamination and splitting in composite materials and its application to scaled notched tensile specimens," *International journal for numerical methods in engineering,* vol. 69, pp. 1982-1995, 2007.
[34] M. De Moura and J. Gonçalves, "Modelling the interaction between matrix cracking and delamination in carbon–epoxy laminates under low velocity impact," *Composites Science and Technology,* vol. 64, pp. 1021-1027, 2004.
[35] S. Mukhopadhyay, M. I. Jones, and S. R. Hallett, "Compressive failure of laminates containing an embedded wrinkle; experimental and numerical study," *Composites Part A: Applied Science and Manufacturing,* vol. 73, pp. 132-142, 2015.
[36] S. Mukhopadhyay, M. I. Jones, and S. R. Hallett, "Tensile failure of laminates containing an embedded wrinkle; numerical and experimental study," *Composites Part A: Applied Science and Manufacturing,* vol. 77, pp. 219-228, 2015.
[37] N. Moës and T. Belytschko, "Extended finite element method for cohesive crack growth," *Engineering fracture mechanics,* vol. 69, pp. 813-833, 2002.
[38] C. Ye, J. Shi, and G. J. Cheng, "An eXtended Finite Element Method (XFEM) study on the effect of reinforcing particles on the crack propagation behavior in a metal–matrix composite," *International Journal of Fatigue,* vol. 44, pp. 151-156, 2012.
[39] A. Melro, P. Camanho, F. A. Pires, and S. Pinho, "Micromechanical analysis of polymer composites reinforced by unidirectional fibres: Part II–Micromechanical analyses," *International Journal of Solids and Structures,* vol. 50, pp. 1906-1915, 2013.
[40] A. Melro, P. Camanho, and S. Pinho, "Generation of random distribution of fibres in long-fibre reinforced composites," *Composites Science and Technology,* vol. 68, pp. 2092-2102, 2008.
[41] H. Lin, L. P. Brown, and A. C. Long, "Modelling and Simulating Textile Structures Using TexGen," *Advanced Materials Research,* vol. 331, pp. 44-47, 2011.
[42] S. V. Lomov, D. S. Ivanov, I. Verpoest, M. Zako, T. Kurashiki, H. Nakai*, et al.*, "Meso-FE modelling of textile composites: Road map, data flow and algorithms," *Composites Science and Technology,* vol. 67, pp. 1870-1891, 2007.
[43] S. Tabatabaei and S. V. Lomov, "Eliminating the volume redundancy of embedded elements and yarn interpenetrations in meso-finite element modelling of textile composites," *Computers & Structures,* vol. 152, pp. 142-154, 2015.
[44] S. Tabatabaei, S. V. Lomov, and I. Verpoest, "Assessment of embedded element technique in meso-FE modelling of fibre reinforced composites," *Composite Structures,* vol. 107, pp. 436-446, 2014.
[45] W.-G. Jiang, S. R. Hallett, and M. R. Wisnom, "Development of domain superposition technique for the modelling of woven fabric composites," in *Mechanical response of composites*, ed: Springer, 2008, pp. 281-291.
[46] H. Bale, M. Blacklock, M. R. Begley, D. B. Marshall, B. N. Cox, and R. O. Ritchie, "Characterizing Three-Dimensional Textile Ceramic Composites Using Synchrotron X-Ray Micro-Computed-Tomography," *Journal of the American Ceramic Society,* vol. 95, pp. 392-402, 2012.
[47] I. Straumit, S. V. Lomov, and M. Wevers, "Quantification of the internal structure and automatic generation of voxel models of textile composites from X-ray computed tomography data," *Composites Part A: Applied Science and Manufacturing,* vol. 69, pp. 150-158, 2015.
[48] Y. Mahadik, K. A. Brown, and S. R. Hallett, "Characterisation of 3D woven composite internal architecture and effect of compaction," *Composites Part A: Applied Science and Manufacturing,* vol. 41, pp. 872-880, 2010.
[49] D. Durville, "Simulation of the mechanical behaviour of woven fabrics at the scale of fibers," *International journal of material forming,* vol. 3, pp. 1241-1251, 2010.
[50] G. Zhou, X. Sun, and Y. Wang, "Multi-chain digital element analysis in textile mechanics," *Composites science and Technology,* vol. 64, pp. 239-244, 2004.
[51] J. Gager and H. E. Pettermann, "Numerical homogenization of textile composites based on shell element discretization," *Composites Science and Technology,* vol. 72, pp. 806-812, 2012.
[52] P. Badel, E. Vidal-Sallé, and P. Boisse, "Large deformation analysis of fibrous materials using rate constitutive equations," *Computers & Structures,* vol. 86, pp. 1164-1175, 2008.
[53] G. Hivet and P. Boisse, "Consistent mesoscopic mechanical behaviour model for woven composite reinforcements in biaxial tension," *Composites Part B: Engineering,* vol. 39, pp. 345-361, 2008.
[54] M. A. Khan, T. Mabrouki, E. Vidal-Salle, and P. Boisse, "Numerical and experimental analyses of woven composite reinforcement forming using a hypoelastic behaviour. Application to the double dome benchmark," *Journal of Materials Processing Technology,* vol. 210, pp. 378-388, 2010.
[55] F. Stig and S. Hallström, "Spatial modelling of 3D-woven textiles," *Composite Structures,* 2011.
[56] C. C. Chamis, "Simplified composite micromechanics equations for hygral, thermal and mechanical properties," 1983.

[57] CGAL. *Computationl Geomtrey Algorithms Library*. Available: http://www.cgal.org
[58] S. Green, M. Matveev, A. Long, D. Ivanov, and S. Hallett, "Mechanical modelling of 3D woven composites considering realistic unit cell geometry," *Composite Structures,* vol. 118, pp. 284-293, 2014.
[59] S. Balay, K. Buschelman, D. Gropp, D. Kaushik, G. Knepley, C. Mcinnes*, et al.*, "{PETSc}{W} eb page," 2001.
[60] S. Balay, J. Brown, K. Buschelman, V. Eijkhout, W. Gropp, D. Kaushik*, et al.*, "PETSc Users Manual Revision 3.4," 2013.
[61] J. Schneider, G. Hello, Z. Aboura, M. Benzeggagh, and D. Marsal, "A meso-FE voxel model of an interlock woven composite," in *Proceeding of the international conference in composite materials 17th (ICCM17), Edinburgh, Scotland*, 2009.
[62] E. Potter, S. Pinho, P. Robinson, L. Iannucci, and A. McMillan, "Mesh generation and geometrical modelling of 3D woven composites with variable tow cross-sections," *Computational Materials Science,* vol. 51, pp. 103-111, 2012.
[63] I. Verpoest and S. V. Lomov, "Virtual textile composites software WiseTex: Integration with micro-mechanical, permeability and structural analysis," *Composites Science and Technology,* vol. 65, pp. 2563-2574, 2005.
[64] S. Ghosh and S. Moorthy, "Elastic-plastic analysis of arbitrary heterogeneous materials with the Voronoi cell finite element method," *Computer Methods in Applied Mechanics and Engineering,* vol. 121, pp. 373-409, 1995.
[65] S. Ghosh, K. Lee, and S. Moorthy, "Multiple scale analysis of heterogeneous elastic structures using homogenization theory and Voronoi cell finite element method," *International Journal of Solids and Structures,* vol. 32, pp. 27-62, 1995.
[66] S. Ghosh, K. Lee, and S. Moorthy, "Two scale analysis of heterogeneous elastic-plastic materials with asymptotic homogenization and Voronoi cell finite element model," *Computer Methods in Applied Mechanics and Engineering,* vol. 132, pp. 63-116, 1996.
[67] A. Okabe, B. Boots, K. Sugihara, and S. N. Chiu, *Spatial tessellations: concepts and applications of Voronoi diagrams* vol. 501: John Wiley & Sons, 2009.
[68] D. O. Adams, J. M. Moriarty, A. M. Gallegos, and D. F. Adams, "The V-notched rail shear test," *Journal of composite materials,* vol. 41, pp. 281-297, 2007.
[69] C. Farhat, K. Pierson, and M. Lesoinne, "The second generation FETI methods and their application to the parallel solution of large-scale linear and geometrically non-linear structural analysis problems," *Computer methods in applied mechanics and engineering,* vol. 184, pp. 333-374, 2000.
[70] J. Xu, B. N. Cox, M. McGlockton, and W. Carter, "A binary model of textile composites—II. The elastic regime," *Acta metallurgica et materialia,* vol. 43, pp. 3511-3524, 1995.
[71] B. Cox, W. Carter, and N. Fleck, "A binary model of textile composites—I. Formulation," *Acta metallurgica et materialia,* vol. 42, pp. 3463-3479, 1994.
[72] P. Tan, L. Tong, and G. Steven, "Behavior of 3D orthogonal woven CFRP composites. Part II. FEA and analytical modeling approaches," *Composites Part A: Applied Science and Manufacturing,* vol. 31, pp. 273-281, 2000.